Journal of Luminescence 263 (2023) 120158

Contents lists available at ScienceDirect

Journal of Luminescence

journal homepage: www.elsevier.com/locate/jlumin

The influence of imidazolium counterions on the luminescence properties of $C_n$mim[Eu(tta)$_4$] tetrakis complexes in solid-state and ionic liquid solutions

Tiago B. Paolini [a], Israel P. Assunção [a,b], Israel F. Costa [a], Lucca Blois [a], Maria Cláudia F.C. Felinto [c], Renaldo T. Moura Jr. [d,e], Ercules E.S. Teotonio [f], Oscar L. Malta [g], Albano N. Carneiro Neto [h,**], Hermi F. Brito [a,*]

[a] Department of Fundamental Chemistry, Institute of Chemistry, University of São Paulo, 05508-000, São Paulo, SP, Brazil
[b] Education, Science, and Technology Federal Institute of São Paulo, São Paulo, 01109-010, Brazil
[c] Nuclear and Energy Research Institute – IPEN/CNEN, 05508-000, São Paulo, SP, Brazil
[d] Computational and Theoretical Chemistry Group (CATCO), Department of Chemistry, Southern Methodist University Dallas, TX, 75275, USA
[e] Department of Chemistry and Physics Center of Agrarian Sciences, Federal University of Paraiba, Areia, PB, 58397-000, Brazil
[f] Department of Chemistry, Federal University of Paraíba, 58051-970, João Pessoa, PB, Brazil
[g] Departamento de Química Fundamental, Universidade Federal de Pernambuco, Recife, PE, Brazil
[h] Physics Department and CICECO – Aveiro Institute of Materials, University of Aveiro, Aveiro, Portugal

ARTICLE INFO

Keywords:
Photoluminescence
Ln^{3+} tetrakis complexes
Imidazolium-based ionic liquids
Microwave-assisted method
Energy transfer

ABSTRACT

A series of lanthanide tetrakis complexes $C_n$mim[Ln(tta)$_4$] where Ln^{3+}: Eu^{3+} and Gd^{3+}, $C_n$mim: imidazolium-based counterions (n from 3 to 8) and tta: thenoyltrifluoroacetonate were synthesized by a one-pot method. The $C_n$mim[Ln(tta)$_4$] complexes are thermostable up to 210 °C and present an isomorphic-like character for the complexes with n = 5, 6, and 7. The phosphorescence spectral profile of the $C_n$mim[Gd(tta)$_4$] complexes showed intense emission broadbands, in which the barycenters are slightly shifted to energies from the 18,950 to 18,450 cm^{-1} range. The $C_n$mim[Eu(tta)$_4$] complexes in solutions of the corresponding [$C_n$mim]Br ionic liquids show similar emission spectral profiles as their corresponding in the solid state, indicating that the coordination polyhedron does not undergo a significant variation when the chemical environment is changed. Relatively high values of the intensity parameter Ω_2 in both media are presented. The Ω_4 values of the complexes in solutions of ionic liquids are also similar, reinforcing that there are small changes in the polyhedral coordination from the solid state to the ionic liquid solution. The series presents high intrinsic emission quantum efficiencies, $90\% \geq q_{Eu}^{Eu} \geq 53\%$. In addition, theoretical calculations on the intramolecular energy transfer (IET) reveal the participation of the $^7F_0 \rightarrow {}^5D_1$ and $^7F_1 \rightarrow {}^5G_2$ transitions for the IET via S_1 while the IET via T_1 state is dominated by the $^7F_0 \rightarrow {}^5D_1$ and $^7F_1 \rightarrow {}^5D_0$ transitions. Therefore, due to their high luminescent features, these Eu^{3+} tetrakis complexes are potential candidates to be applied as optical markers in the solid-state or even in ionic liquid solutions.

1. Introduction

Due to the forbidden nature of the 4f-4f transitions, Ln^{3+} ions present very low molar absorptivity coefficients and emission intensity under direct excitation. This drawback is usually overcome by using luminophores (or sensitizers) that absorb and efficiently transfer the energy to the Ln^{3+} that afterward emits according to its energy level structure and selection rules on *J* quantum number [1,2]. In coordination compounds, the luminescence sensitizer [3] are usually organic ligands, and among them, the β-diketones are the most widely used [4–10]. The sensitizing process generally occurs via the strong light absorption by the ligand from the ground to excited singlet states ($S_0 \rightarrow S_n$), then, the population of the S_1 state can decay non-radiatively to a lower excited ligand triplet state ($S_1 \rightarrow T_1$), a process known as intersystem crossing [11–13]. Next,

* Corresponding author.
** Corresponding author.
E-mail addresses: albanoneto@ua.pt (A.N. Carneiro Neto), hefbrito@iq.usp.br (H.F. Brito).

https://doi.org/10.1016/j.jlumin.2023.120158
Received 4 March 2023; Received in revised form 22 August 2023; Accepted 28 August 2023
Available online 29 August 2023

the T_1 state can transfer the energy to the lanthanide ion ($T_1 \rightarrow Ln^{3+}$) that may decay radiatively according to its intrinsic energy level structures [14,15]. It is noteworthy that the intramolecular energy transfer may eventually occur directly from S_1 to high energy levels of the Ln^{3+} ion [16–19]. In addition, deactivation pathways can significantly quench the luminescence intensity via coupling with high-energy oscillators such as C–H, N–H, and mainly O–H [20–22].

To improve the luminescence efficiency and avoid such shortcomings, the Ln^{3+} tetrakis-complexes $Q[Ln(L)_4]$ are an interesting choice, once four ligands around the Ln^{3+} ion virtually saturate its first coordination sphere and the addition of one more of the same ligand in comparison to those Ln^{3+} tris-complexes (*e.g.*, $[Ln(L)_3(H_2O)_x]$). The $[Ln(L)_4]^-$ moieties are usually anionic and thus, a counterion Q^+ must be present for the compound to remain neutral in charge. The most applied counterions are organic-based such as alkyl and phenyl groups [23–25], pyrrolidinium [26], piperidinium [26], pyridinium [27], and imidazolium [28,29]. However, alkali metal ions (Li^+, Na^+, K^+, Rb^+) can be used as well [30–32].

It is noteworthy that ionic liquids are defined as organic salts with low melting points [33–35] (usually below 373 K) that present high thermal and electrochemical stability, negligible volatility, high polarity, and electrical conductivity. They comprise many different classes including quaternary ammonium and phosphonium, pyridinium, pyrrolidinium, and mainly imidazolium-based salts, including those with the Ln^{3+} ions [36–40]. In addition, these compounds are considered excellent green solvents for reactions [33,41–43].

The present work reports the one-pot synthesis and photoluminescence properties of a new series of Eu^{3+} and Gd^{3+} tetrakis-complexes with thenoyltrifluoroacetonate (tta) ligand and imidazolium-based counterions ($C_n$mim with n from 3 to 8), as illustrated in Fig. 1. The spectroscopic properties of these complexes were investigated either in the solid state or dissolved in imidazolium-based ionic liquids, $[C_n$mim]Br. Theoretical calculations on the intramolecular energy transfer (IET) rates were also performed for the solid-state complexes in the JOYSpectra web platform [44]. The photoluminescence results indicated that these $C_n$mim$[Eu(tta)_4]$ complexes can be applied as molecular light emitters.

2. Experimental procedure

Synthesis of $[C_n$mim] Br ionic liquids - The synthetic route was based on reference [45] with some modifications. Toluene was chosen as a solvent, once the alkyl bromide and 1-methylimidazole are both soluble in the reaction media, while the formed ionic liquid is not, then, the final product can be separated by filtration. The molar ratio between the reactants was 1:1 and the average reaction time in the domestic microwave oven was 15 min. Afterward, the heterogeneous mixture was transferred to a regular hot plate and heated at 60 °C until the complete removal of the solvent. All ionic liquids were formed as viscous yellowish oils at room temperature and the average yields were about 75%. It is worth mentioning that the microwave-assisted method presents some advantages over more traditional synthetic routes such as reduction of energy consumption, shorter reaction time, and higher product yield.

Synthesis of $C_n$mim $[Ln(tta)_4]$ tetrakis complexes - Firstly, the precursor Ln^{3+} chlorides (Ln^{3+}: Eu and Gd) were synthesized according to the literature [46] by the reaction of the corresponding Ln_2O_3 with HCl (37% w/w). The $C_n$mim$[Ln(tta)_4]$ complexes were synthesized according to Refs. [7,47], by a one-pot method. Nevertheless, isopropanol was used instead of EtOH, the source of ionic liquid was a bromide, and the molar ratio of ligand:counterion:Ln^{3+} was 5:3/2:1. The organic ligand was previously deprotonated with a 1.0 mol•L^{-1} $NaOH_{(aq)}$ solution and the respective $LnCl_3$•$6H_2O$ was added dropwise to a 3:1(v/v) homogeneous EtOH/H_2O mixture containing the ligand and the $[C_n$mim]Br, with n = 3, 4, 5, 6, 7, and 8. The solution was stirred for 3 h at 50 °C until the evaporation of the isopropanol. Subsequently, the solid product was filtered, washed with distilled water, dried, and stored under reduced pressure in a desiccator. The overall average yield was ~90%.

Instrumental techniques - The elemental analyses were performed in PerkinElmer CHN 2400 instruments. Thermogravimetric curves (TG/DTG) were performed in the 25–900 °C range on a thermobalance SHIMADZU equipment model TGA-51 under a dynamic synthetic air atmosphere of 50 cm^3•min^{-1} with a constant heating rate of 10 °C•min^{-1}. Differential scanning calorimetry (DSC) curves were registered in a Shimadzu DSC-50 cell using aluminum crucibles, under a dynamic $N_{2(g)}$ atmosphere (100 cm^3•min^{-1}) and a heating rate of 10 °C•min^{-1} in the temperature range from 25 to 600 °C. Still, the cell was calibrated with indium (m.p. 156.6 °C; $\Delta H_{fus.}$ = 28.54 J•g^{-1}) and zinc (m.p. 419.6 °C) with 99.9% of purity. FTIR spectra were measured with a Bomem MB102 FTIR spectrometer in the 4,000 to 400 cm^{-1} range with a spectral resolution of 4.0 cm^{-1} using KBr pellets. Proton nuclear magnetic resonance (^{1}H NMR) was registered in a 300 MHz Bruker spectrometer using $CDCl_3$ as solvent and tetramethylsilane (TMS) as the internal reference. X-ray diffraction patterns were registered with a Miniflex Rigaku diffractometer using CuKα1 radiation (30 kV and 15 mA) in the (2θ) 5–60° range and of 0.02 s of pass time. The excitation and emission spectra of the Ln^{3+} tetrakis complexes in the solid state were recorded at room (300 K) and liquid nitrogen (77 K) temperatures at an angle of 22.5° (front face) with a spectrofluorometer (SPEX-Fluorolog 3) with double grating between 0.5 and 2.0 mm monochromator (SPEX1680), and the excitation source was a 450 W Xenon lamp. The photoluminescent measurements of the ionic liquid solutions (at 1% mol) of the $C_n$mim$[Eu(tta)_4]$ complexes were performed under the same instrumental conditions, but only at room temperature. Besides, all spectra were recorded using a detector mode correction. Moreover, the

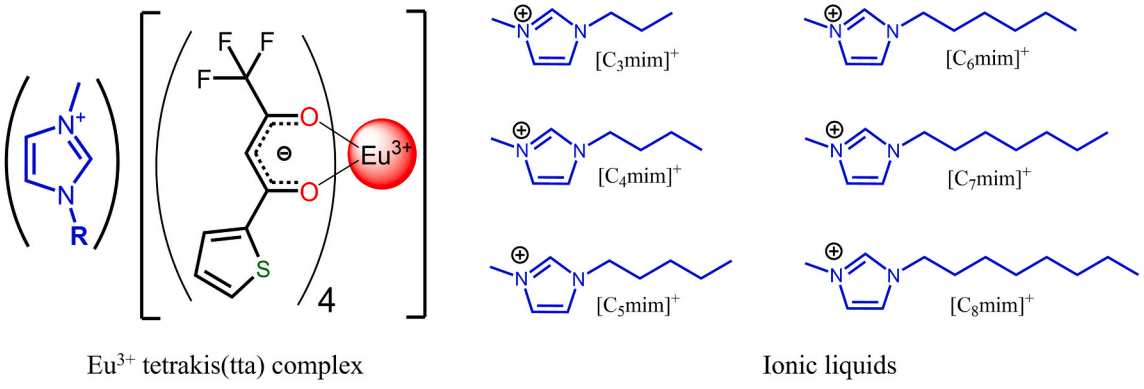

Fig. 1. Chemical structure of $C_n$mim$[Eu(tta)_4]$ tetrakis complexes (left) with $[C_n$mim$]^+$ ionic liquids as counterions (right), where R stands for an aliphatic chain (n = 3, 4, 5, 6, 7 and 8).

luminescence decay curves of the emitting levels of the Eu^{3+} ions complexes were obtained at room temperature, using a phosphorimeter SPEX 1934D accessory coupled to the spectrofluorometer.

3. Results and discussion

Elemental analysis of C, H, N, and Br contents for the ionic liquids [$C_n$mim]Br, where n = 4, 5, and 7 are consistent with the expected stoichiometry *i.e.*, ($C_8H_{15}N_2$)Br, ($C_9H_{17}N_2$)Br and ($C_{11}H_{21}N_2$)Br (Table S2 in the Supporting Information). In addition, proton nuclear magnetic resonance (^{1}H NMR) spectra of these ionic liquids (Figs. S1a–c in the Supporting Information) showed peaks in good agreement with previous data [48,49]. The peaks located at δ 0.9 (triplet), 1.3 (multiplet), 1.9 (quintet), and 4.3 (triplet) were attributed to the protons from the alkyl groups bonded to nitrogen 3, while the 4.1 ppm peak is referent to CH_3 group attached to the nitrogen 1 of the imidazole ring. The protons related to carbon atoms 2, 4, and 5 in the ring are located, respectively, at δ 10.2 (singlet); 7.5 (triplet), and 7.6 (triplet). The proper location of such peaks indicated the ionic liquids were successfully synthesized. Elemental analysis (CHN) data of the Ln^{3+}-complexes also agree with anhydrous tetrakis species containing imidazolium-based ionic liquids as countercations, suggesting the general formula $C_n$mim[Ln(tta)$_4$], where n = 3, 4, 5, 6, 7, and 8 (Table S1 in the Supporting Information).

Thermogravimetric analysis (TG/DTG and DSC) of the $C_n$mim[Eu(tta)$_4$] complexes revealed the same thermal behavior for all tetrakis complexes (Fig. S2 in the Supporting Information). In general, TG curves and their corresponding DTG (solid and dashed black lines in Fig. S2, respectively) indicate no weight loss in the temperature interval from 25 to 210 °C for all anhydrous $C_n$mim[Eu(tta)$_4$] complexes, suggesting that all investigated $C_n$mim[Eu(tta)$_4$] complexes are thermally stable. Besides, from 115 to 140 °C, the DSC curves (solid red lines in Fig. S2) showed endothermic events without mass variation, which points toward a phase transition process. The decomposition events start around 210 °C in two distinct exothermic steps. In the first one, between 240 and 300 °C, the weight loss corresponds to [$C_n$mim]$^+$ counterion and one single tta anion, possibly leading to the tris-complexes species. The second event takes place in the 300–600 °C interval and corresponds to the loss of the remaining tta ligands. Finally, the mass increase in the exothermic events from 610 to 860 °C, corresponds to the oxidation of the sulfur atom from the tta ligand to sulfate and the consequent formation of a final residue of europium (III) fluorosulfate, $EuF(SO_4)$. This thermal result was also confirmed by a test with an aqueous solution of $BaCl_2$, indicating the presence of sulfate ions.

The $C_n$mim[Eu(tta)$_4$] compounds were also characterized by FTIR spectroscopy that showed the high absorption band at 1,607 cm^{-1} (Fig. S3 in the Supporting Information) assigned to the carbonyl symmetric stretching mode ν_s(C=O). Once this band is shifted to lower energies compared to the free Htta ligand (~1,660 cm^{-1}) [50], we can infer the effective coordination of the tta ligand to the Eu^{3+} ion through a bidentate chelate mode [51]. The low-intensity band around 460 cm^{-1} corresponds to the Ln–O stretching mode, also indicating the ligand coordination to the Eu^{3+} ion through the β-diketone carbonyl groups. The spectral profile of all members in the series is very similar to each other regardless of the chain length of the [$C_n$mim]$^+$ cations, revealing their small influence on the metal ion coordination. It is worth mentioning that the broad absorption band in the spectral range of 3,700 to 3,200 cm^{-1} (Fig. S3) is attributed to the moisture adsorption by the KBr pellets.

In general, X-ray powder diffraction (XPD) patterns of the $C_n$mim[Eu(tta)$_4$] (Fig. 2) reveal relatively low-intensity peaks, suggesting small crystallinity. A possible explanation is a counterion long and flexible chain that prevents a suitable approximation between each complex entity and an ordered packing. Interestingly, this observation is in complete opposition to other tetrakis β-diketonates such as acetylacetone-based ones containing alkaline metals as counterions

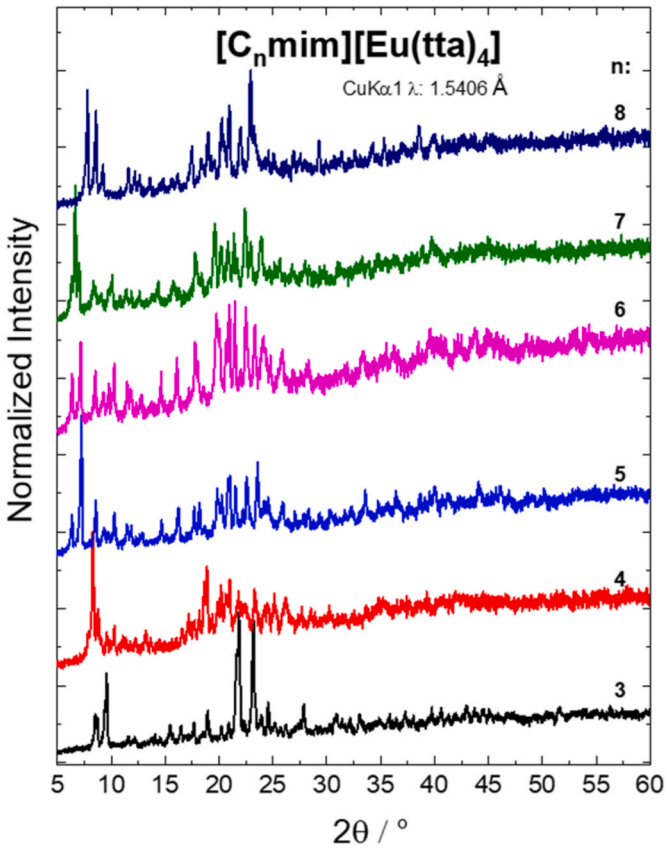

Fig. 2. X-Ray powder diffraction pattern (XPD) of the $C_n$mim[Eu(tta)$_4$] complexes where n = 3 to 8. All diffractograms were recorded at room temperature in the 5–60° range.

[52]. Nevertheless, the C_3mim[Eu(tta)$_4$] complex presents the highest crystallinity among the series, with the most intense peaks in the 20 to 25°, which can be due to the smaller chain length of the [C_3mim]$^+$ species. Also, the complexes with countercations with 5, 6, and 7 carbon atoms present diffraction patterns with significant similarity, suggesting an isomorphic-like character. On the other hand, the complexes with [C_3mim]$^+$, [C_4mim]$^+$, and [C_8mim]$^+$ counterions present the most distinctive structures among themselves and the other series members (Fig. 2).

4. Luminescent properties

4.1. Photoluminescence of the [$C_n$mim]Br ionic liquids

Excitation spectra of the [$C_n$mim]Br ionic liquids (n = 4, 5, and 7) were obtained at 300 K, monitoring the emission at 560 nm in the 200–540 nm range (Fig. S4a in the Supporting Information). All spectra present broad excitation bands with a small influence on the carbon chain length, leading to similar profiles, although the [C_7mim]Br is slightly broader than [C_4mim]Br and [C_5mim]Br salts. Similarly, the corresponding emission spectra were also recorded with excitation at 350 nm, in the 370–730 nm range (Fig. S4b). The systems with n = 5 and 7 present higher similarities in their spectral profile compared to the [C_4mim]Br species that show a significant shift to higher energies. This spectral shape difference is attributed to the dependence on the excitation wavelength, as demonstrated by S. Cha et al. [53]. This study discusses the impact of intermolecular interactions on the emission of [C_4mim][BF_4] ionic liquids. These interactions may result in variations when the carbon chain size is altered (*e.g.*, [C_5mim]$^+$ and [C_6mim]$^+$).

4.2. Time-resolved phosphorescence of the $C_n$mim[Gd(tta)$_4$] complexes

The Gd^{3+} ion is optically inactive for wavelengths above 315 nm due to the large energy gap between the ground state $^8S_{7/2}$ ground state and the first $^6P_{7/2}$ excited state (ca. 32,000 cm^{-1}) [54], which is often higher than the majority of the organic ligand triplet states (T_1). In addition, Gd^{3+} and Eu^{3+} have a similar ionic radius and thus, Gd^{3+} complexes can mimic the chemical environment of the analog Eu^{3+} complexes [55,56]. To avoid possible contributions from the $S_1 \rightarrow S_0$ transition that can be overlapped with the tta phosphorescence band ($T_1 \rightarrow S_0$), the phosphorescence spectra (Fig. 3) of the $C_n$mim[Gd(tta)$_4$] complexes (n = 3 to 8) were registered with a time delay of 1 ms. The low-temperature (77 K) emission spectra, recorded in the 400–750 nm range under excitation at 380 nm, revealed a broad phosphorescence band assigned to the $T_1 \rightarrow S_0$ transition from tta ligands. It is noteworthy that contributions from the $[C_n mim]^+$ cations were not observed, indicating the central role of the tta ligand as a donor in the intramolecular energy transfer (IET) process in these tetrakis complexes (Fig. 4). Such results can be explained due to the presence of β-diketonate in the first coordination sphere of the metal ion.

The energy positions of the ligand T_1 states were determined based on the barycenter of the phosphorescence band and the results are summarized in Table S3. Interestingly, the energies of the barycenters are not significantly affected by the carbon chain size of the imidazolium-based cations with an average value of 18,624 cm^{-1}. Therefore, based on these experimental results and the relative position of the Eu^{3+} energy levels [54], *e.g.*, $^5D_1$ (19,050 cm^{-1}) and $^5D_0$ (17,290 cm^{-1}), it is possible to infer that a $T_1 \rightarrow Eu^{3+}$ energy transfer can play a central role in the luminescence sensitization process, as will be detailed in the next section.

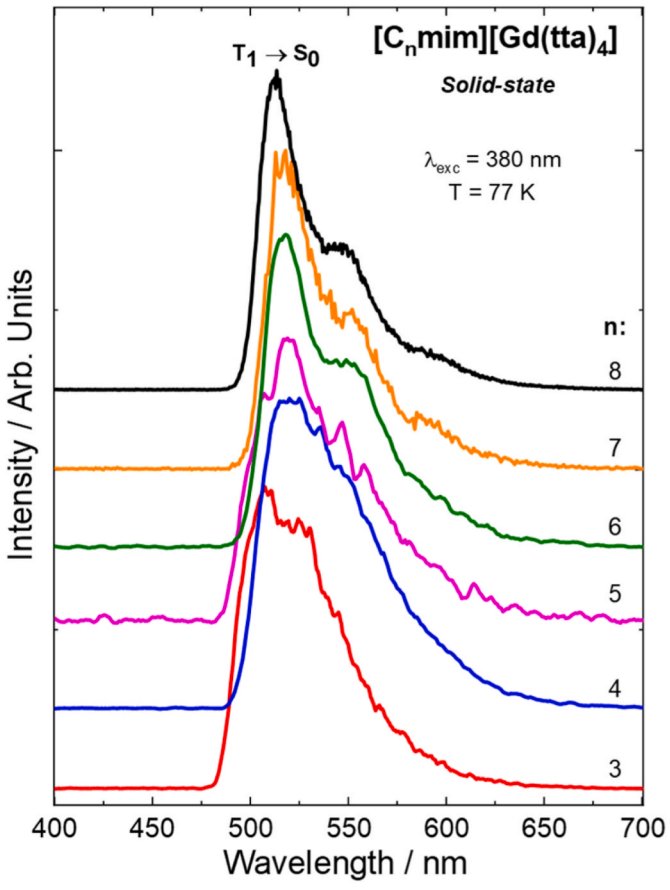

Fig. 3. Time-resolved phosphorescence spectra of the $C_n$mim[Gd(tta)$_4$] complexes, where (n = 3 to 8). The spectra were registered under 77 K from 400 to 700 nm with excitation at 381 nm with a delay of 1 ms.

In general, the T_1 energy position can be obtained using either the zero-phonon line or the barycenter. The barycenter is particularly valuable in spectroscopy as it provides a straightforward and intuitive measure of the band position. It is also less susceptible to noise and baseline fluctuations compared to other measures such as the maximum peak or zero-phonon line. Furthermore, the barycenter remains unaffected by temperature [57]. It is widely employed in spectral analysis and the study of intramolecular energy transfer [1]. This allows for the consideration of other Franck-Condon transitions [1,58], which may be more resonant with the acceptor transition and thus make a greater contribution to the energy transfer process than the zero-phonon transition.

4.3. Photoluminescence of the $C_n$mim[Eu(tta)$_4$] complexes

The excitation spectra of the $C_n$mim[Eu(tta)$_4$] tetrakis complexes in solid state (Fig. 4a) and [$C_n$mim]Br ionic liquid solutions (n = 3 to 8) were registered at room temperature in the 250–575 nm range monitoring the emission at the $^5D_0 \rightarrow {}^7F_2$ transition (616 nm) of the Eu^{3+} ion (Fig. 4b). The spectra revealed a broad excitation intensity band from 250 to 450 nm assigned to the $S_0 \rightarrow S_1$ transition centered on the tta ligand. Besides, some narrow excitation peaks can also be seen at 395, 464, 526, and 535 nm assigned to the $^7F_0 \rightarrow {}^5L_6$, $^7F_0 \rightarrow {}^5D_2$, $^7F_0 \rightarrow {}^5D_1$, and $^7F_1 \rightarrow {}^5D_1$ transitions of the Eu^{3+} ion, respectively. The low-temperature (77 K) spectral profiles of the Eu^{3+}-complexes (Fig. S5 in the Supporting Information) showed small differences when compared to the analogous room-temperature ones. The most significant change is the $^7F_1 \rightarrow {}^5D_1$ transition vanishes at low temperatures. This observation is in agreement with the thermally coupled populations of the $^7F_1$ and $^7F_0$ levels [59,60]. The former can be thermally populated, although, at low temperatures, the $^7F_0 \rightarrow {}^5D_1$ transition is more likely to occur [61]. Also, the low-temperature spectra (Fig. S5) as expected presents higher resolution.

The emission spectra of the Eu^{3+} tetrakis complexes and the corresponding [$C_n$mim]Br solutions were registered at 300 K in the 570–720 nm range under excitation at 395 nm. As observed in Fig. 5a, both spectra revealed only narrow emission peaks attributed mainly to the $^5D_0 \rightarrow {}^7F_{0\text{-}4}$ transitions of the Eu^{3+} ions [54], with the $^5D_0 \rightarrow {}^7F_2$ as the most intense one and the main responsible for the bright red emission of these coordination compounds (Fig. 5a and b). It is noteworthy that the electronic transitions of the europium complexes in the solution (Fig. 5b) are more broadened than those in solid-sate (Fig. 5a), reflecting its multisite character caused by the solvent effect. In general, no emission broadband arising from the ligands was observed in the spectra either for the solid-state complexes or the corresponding [$C_n$mim]Br solutions, which suggests an efficient intramolecular $L \rightarrow Eu^{3+}$ energy transfer process. Concerning the 77 K emission spectra of the $C_n$mim[Eu(tta)$_4$] complexes, depicted in Fig. S6 (Supporting Information), no appreciable differences were observed in comparison with the spectra recorded at room temperature, except for the higher resolution of the latter in comparison with the former due a lowering in vibronic contributions.

An interesting feature of the emission spectral profiles of the europium tetrakis complexes in solution is their remarkable similarity, irrespective of the countercation carbon chain length. This spectroscopic result indicates that the chemical environment around the Eu^{3+} ion is similar in solution and that the tta ligand is also tetrakis coordinated with the metal ion.

Except for the C_4mim[Eu(tta)$_4$] compound, the presence of just one $^5D_0 \rightarrow {}^7F_0$ emission peak is identified (Fig. S7), indicating a single point symmetry. Nevertheless, Nockemann et al. reported the crystal structure of C_6mim[Eu(tta)$_4$] and identified a single symmetry site [36]. Furthermore, when analyzing the Eu^{3+} $^5D_0$ lifetimes in the studied compounds, the luminescence decay curves are well-fitted by a single-exponential function, also indicating the presence of only one

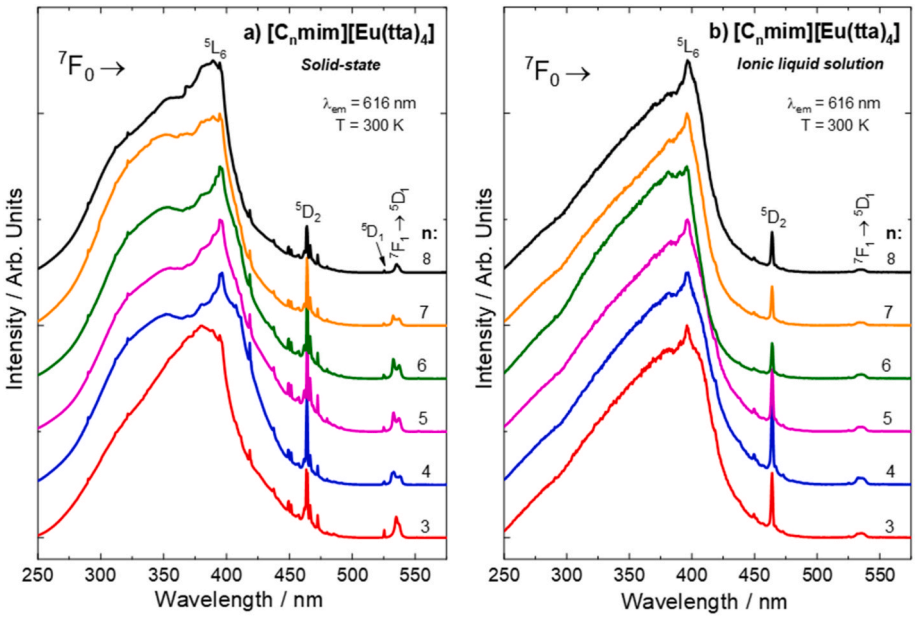

Fig. 4. Excitation spectra of the complexes recorded at room temperature of a) $C_n$mim[Eu(tta)$_4$] in solid state and b) solution at 1% in mol of each [$C_n$mim]Br ionic liquid (n = 3 to 8). The spectra were registered by monitoring the emission at the $^5D_0 \rightarrow {}^7F_2$ transition (616 nm) of the Eu^{3+} ion.

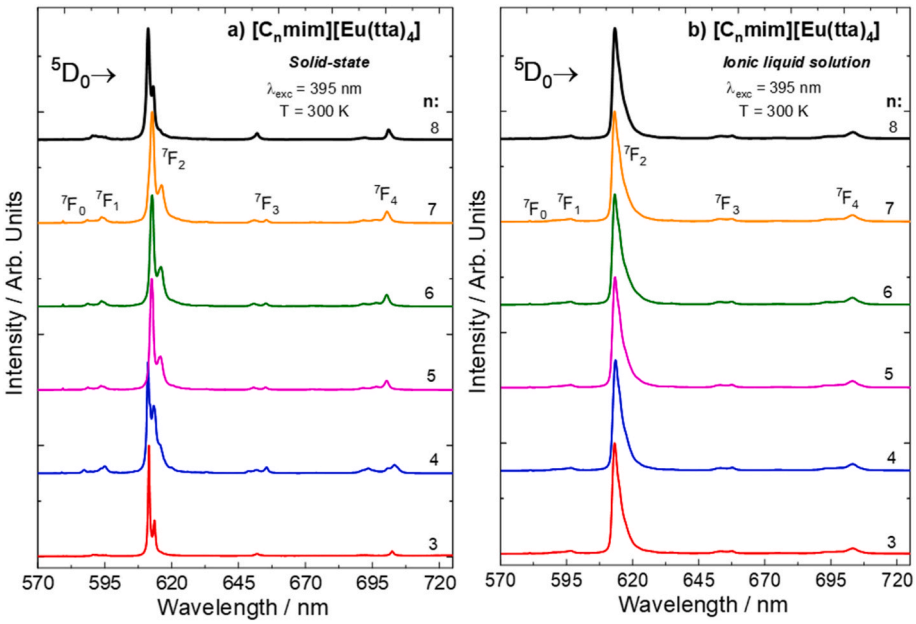

Fig. 5. Emission spectra of the $C_n$mim[Eu(tta)$_4$] complexes recorded at room temperature in the a) solid-state and b) solution at 1% in mol of each [$C_n$mim]Br ionic liquid (n = 3 to 8).

emitting center. It's important to note that the analysis based on the number of peaks in the $^5D_0 \rightarrow {}^7F_0$ transition and the fitting of decay curves can solely provide an indication of the potential number of different Eu^{3+} sites because when the Eu^{3+} is placed within a cubic group (such as D_n, D_{nd}, and D_{nh} point group symmetries [62]), the $^5D_0 \rightarrow {}^7F_0$ transition is not observed.

Interestingly, the C_4mim[Eu(tta)$_4$] complex stands out by displaying two $^5D_0 \rightarrow {}^7F_0$ peaks (Fig. S7), suggesting the potential existence of two different Eu^{3+} centers in this particular compound. A comprehensive investigation into the interaction between these two centers and its impact on luminescent features will be the central focus of a forthcoming study.

It is important to mention that the complexes present a high vibronic contribution due to some lower energy peaks overlapping with those of the $^5D_0 \rightarrow {}^7F_1$ (595 nm) and $^5D_0 \rightarrow {}^7F_2$ (616 nm) transitions. Despite these low-intensity peaks arising from vibronic coupling, the splitting pattern of the $^5D_0 \rightarrow {}^7F_{0,1,2,4}$ transitions of the solid-state $C_n$mim[Eu(tta)$_4$], with n = 5, 6 and 7 present, 1, 2, 2 and 4 peaks, respectively.

The solid-state and solution emission spectra revealed weak intensity peaks attributed to emission from the higher excited state $^5D_1$ to the $^7F_{0\text{-}2}$ multiplets. The relative weak intensity of the $^5D_1 \rightarrow {}^7F_{0\text{-}6}$ compared to those arising from the $^5D_0$ level can be rationalized considering the multiphonon decay from the $^5D_1$ to the $^5D_0$ excited states.

The experimental intensity parameters (Ω_2 and Ω_4) values were calculated for the $C_n$mim[Eu(tta)$_4$] complexes and their solutions in the corresponding ionic liquids at 1% in mol (Table 1) according to Eq. (1):

Table 1
Experimental intensity parameters (Ω_2 and Ω_4), radiative (A_{rad}) and non-radiative (A_{nrad}) decay rates, emission lifetime (τ_{obs}), and intrinsic quantum yield (Q_{Eu}^{Eu}) of the solid-state $C_n$mim[Eu(tta)$_4$] complexes (n from 3 to 8) and their corresponding [$C_n$mim]Br ionic liquid solutions at 1% in mol. All data were determined at 300 K. The errors in τ_{obs} are less than 10^{-3} ms.

Solid-state	Ω_2 (10^{-20} cm^2)	Ω_4 (10^{-20} cm^2)	A_{rad} (10^2 s^{-1})	A_{nrad} (10^2 s^{-1})	τ_{obs} (ms)	Q_{Eu}^{Eu} (%)
C_3mim[Eu(tta)$_4$]	33 ± 1	6 ± 1	11.8 ± 0.5	4.1 ± 0.5	0.636	74 ± 2
C_4mim[Eu(tta)$_4$]	32 ± 2	6 ± 1	11.5 ± 0.5	3.7 ± 0.5	0.658	76 ± 3
C_5mim[Eu(tta)$_4$]	42 ± 2	8 ± 1	14.7 ± 0.5	4.5 ± 0.5	0.521	76 ± 3
C_6mim[Eu(tta)$_4$]	44 ± 2	9 ± 1	15.7 ± 0.5	4.0 ± 0.5	0.508	80 ± 2
C_7mim[Eu(tta)$_4$]	45 ± 1	9 ± 1	15.9 ± 0.5	1.8 ± 0.5	0.568	90 ± 3
C_8mim[Eu(tta)$_4$]	39 ± 1	6 ± 1	13.9 ± 0.5	1.7 ± 0.5	0.642	89 ± 3
Solution						
C_3mim[Eu(tta)$_4$]	43 ± 4	8 ± 2	15.4 ± 0.6	13.8 ± 0.6	0.343	53 ± 2
C_4mim[Eu(tta)$_4$]	49 ± 5	10 ± 2	17.2 ± 0.6	4.0 ± 0.6	0.474	81 ± 3
C_5mim[Eu(tta)$_4$]	37 ± 4	7 ± 1	13.3 ± 0.6	11.4 ± 0.6	0.404	54 ± 3
C_6mim[Eu(tta)$_4$]	44 ± 3	9 ± 2	15.8 ± 0.6	12.0 ± 0.6	0.360	57 ± 3
C_7mim[Eu(tta)$_4$]	44 ± 2	10 ± 2	18.0 ± 0.6	2.9 ± 0.6	0.478	86 ± 2
C_8mim[Eu(tta)$_4$]	35 ± 3	9 ± 1	12.8 ± 0.6	6.2 ± 0.6	0.525	67 ± 2

$$A_{0\to\lambda} = \frac{4\omega^3 e^2 \chi}{3\hbar c^3}\Omega_\lambda \langle {}^5D_0 || U^{(\lambda)} || {}^7F_\lambda \rangle^2 \quad (1)$$

where ω is the angular frequency of the transition, e is the elementary charge, $\hbar$ is the reduced Planck's constant, and c is the speed of light. $\chi = (n_{ref}/9)(n_{ref}^2+2)^2$ is the Lorentz local field correction factor, where n_{ref} is the refractive index of the medium. The term $\langle {}^5D_0 || U^{(\lambda)} || {}^7F_\lambda \rangle^2$ are the squared reduced matrix elements whose values are equal to 0.0032 and 0.0023 for λ = 2 and 4, respectively [63]. The χ value was calculated considering n_{ref} = 1.5, a commonly adopted refractive index for lanthanide chelates as found in the literature [1,31,64,65]. In the context of the ionic liquid medium, we determined the n_{ref} values for all samples using an ATAGO™ NAR-3T Abbe Refractometer (Table S5). These findings revealed that the n_{ref} values for [$C_n$mim]Br ionic liquid solutions (at 1% concentration in mol) are slightly lower than those considered for the solid-state. Consequently, the differences observed in the radiative rates (A_{rad}) between the samples in solution and their solid-state counterparts (Table 1) can mostly be attributed to slight structural changes within the first coordination sphere, thereby impacting the Ω_λ parameters. It is noteworthy that recent studies showed the Ω_2 values are more sensitive to small azimuthal angular variations, while the Ω_4 values are more sensitive to the covalent character of the Ln–Ligating atom chemical bond [66–68].

Also, the experimental values for the $A_{0\to J}$ spontaneous emission coefficients related to the $^5D_0 \to {}^7F_{0\text{-}4}$ transitions of the Eu^{3+} ion were obtained from the room temperature emission spectra in the solid-state and solution complexes (Table 1) using Eq. (2) [10,69]:

$$A_{0\to J} = \left(\frac{S_{0\to J}}{S_{0\to 1}}\right) A_{0\to 1} \quad (2)$$

where $S_{0\to1}$ and $S_{0\to J}$ correspond to the areas under the emission curves of the $^5D_0 \to {}^7F_1$ and $^5D_0 \to {}^7F_J$, respectively, although the $^5D_0 \to {}^7F_6$ is rarely observed [10]. The $^5D_0 \to {}^7F_1$ transition is almost completely governed by the magnetic dipole (MD) mechanism and its intensity is practically insensitive to the chemical environment around the Eu^{3+} ion and then, the value $A_{0\to1} \approx 50\ s^{-1}$ (setting $n_{ref} = 1.5$) [10] can be used as an internal reference to determine the $A_{0\to J}$ values.

The intrinsic emission quantum yield (Q_{Eu}^{Eu}) [1,10] is defined as the ratio between the radiative (A_{rad}) and the total (A_{total}) decay rates that are given by the sum of radiative and non-radiative (A_{nrad}) rates (Eq. (3)). Likewise, there is a relationship between A_{total} rate, and the emitting level lifetime (τ_{obs}) given by Eq. (4) [1].

$$Q_{Eu}^{Eu} = \frac{A_{rad}}{A_{rad}+A_{nrad}} = \frac{\tau_{obs}}{\tau_{rad}} \quad (3)$$

$$\tau_{obs} = \frac{1}{A_{rad}+A_{nrad}} = \frac{1}{A_{total}} \quad (4)$$

The experimental emission lifetime (τ_{obs}) values of the $^5D_0$ level were obtained for the solid samples and the 1% (mol) solutions with excitation directly on the Eu^{3+} ion at the $^7F_0 \to {}^5D_1$ transition around 526 nm at room temperature (Fig. S7). As above mentioned, the luminescence decay curves can be well-fitted to a single-exponential function, corroborating the emission spectra data that suggests a single site of symmetry around the Eu^{3+} ion (except for n = 4, as discussed previously). The τ_{obs} values present only small variations among the solid-state samples, while when compared to the solution ones, a more significant variation is observed (Table 1).

As can be seen, the Ω_2 and Ω_4 parameter values (33×10^{-20} cm^2 and 6×10^{-20} cm^2, respectively) for the tetrakis solid-state complexes with $[C_3mim]^+$ and $[C_4mim]^+$ counterions (Table 1) are very similar to those of the hydrated europium tris complex $[Eu(tta)_3(H_2O)_2]$ (33×10^{-20} cm^2 and 6×10^{-20} cm^2, respectively) [70], indicating a similar spectral emission ratio between the $^5D_0 \to {}^7F_2$ and $^5D_0 \to {}^7F_4$ transition intensities concerning the $^5D_0 \to {}^7F_1$ transition. On the other hand, the Ω_2 and Ω_4 values increase for the $C_n$mim[Eu(tta)$_4$] complexes (n = 5, 6, 7 and 8) showing higher emission intensity ratios of these transitions compared to the tetrakis systems with counterion n = 3 and 4, except for the Ω_4 parameter when n = 8. Although the $[Eu(tta)_4]^-$ complexes have similar structures (Table S6), even slight changes can have a significant impact on the chemical environment surrounding the Eu^{3+} ion. These changes are reflected in the values of Ω_λ, particularly in Ω_2, which is more sensitive to angular distortions [71]. In addition, the Ω_2 and Ω_4 experimental parameters values for the Eu^{3+} tetrakis complexes dissolved in their corresponding [$C_n$mim]Br ionic liquid solutions present less variation with the carbon chain length increase from 3 to 8, which is different for solid-state complexes (n = 3 to 7). Even though the intensity parameters present a small variation, it is enough to assert that the local structural changes are responsible for their variations.

It is noted that the highest Q_{Eu}^{Eu} values (from 74 to 90%) $C_n$mim[Eu(tta)$_4$] complexes in solid-state with an increase in the carbon chain length from 3 to 8, indicating that the length of the carbon chain in the $[C_nmim]^+$ may protect the Eu^{3+} ion from being influenced by quenching of C–H vibrational modes. This suggestion agrees with the trend of decreasing A_{nrad} as the number of carbon atoms in the counterion increases (Table 1). Just for comparison, the intrinsic quantum yield for the analogous tris complex in solid-state, $[Eu(tta)_3(H_2O)_2]$ is close to 30% [72]. Such experimental discrepancies are mainly due to the absence of coordinated H_2O molecules around the Eu^{3+} ion in the tetrakis species once the high energy oscillators such as O–H usually lead to strong luminescence quenching [20–22]. In general, the Q_{Eu}^{Eu} values of the solution system are lower than those in solid-state due to the solvent effect. Therefore, the europium tetrakis complexes synthesized in solid-state and in ionic liquid solution show much higher luminescence than the Eu^{3+} tris tta-complex, demonstrating their suitable potential as molecular light-converting devices.

According to semi-empirical PM6/Sparkle [73,74] quantum chemistry calculations, the molecular structures of $[Eu(tta)_4]^-$ are quite similar to each other, with only small differences. The root-mean-square

deviations (RMSD) between the $[Eu(tta)_4]^-$ structures are quantified and presented in Table S6. When the RMSD value is lower, the structures are more similar. In this sense, the compounds C_5mim[Eu(tta)$_4$], C_6mim [Eu(tta)$_4$], and C_7mim[Eu(tta)$_4$] have lower RMSD values between each other, suggesting that the change in $[C_n mim]^+$ from n = 5, 6, and 7 does not significantly distort the $[Eu(tta)_4]^-$ structure. Thus, indicating that they may exhibit similar structures and luminescent properties, as shown by the intensity peaks in Fig. 5. In addition, the donor-acceptor distances for both S_1 and T_1 states (R_L in Eqs. S8–S10), which are considered as the distance from the centroid of each tta ligand to the Ln^{3+} center, are approximately 4 Å for solid-state samples (Fig. S10).

The IET rates from tta ligands to the Eu^{3+} ion were calculated using the JOYSpectra web platform [44], where the energies of the $S_0 \leftarrow S_1$ (26, 250 cm^{-1}) and $S_0 \leftarrow T_1$ (18,950–18,450 cm^{-1}, values in Table S3) transitions were accounted as donors localized at the tta ligand. As acceptors, the combination of $^7F_0$ and $^7F_1$ as initial states and $^5D_0$, $^5D_1$, $^5D_2$, $^5D_3$, $^5D_4$, $^5L_6$, $^5L_7$, $^5G_2$, $^5G_3$, $^5G_5$, and $^5G_6$ as final excited states localized at the Eu^{3+} center are considered. In this sense, 32 non-null IET pathways were calculated for each $C_n$mim[Eu(tta)$_4$] compound (n = 3, 4, 5, 6, 7, and 8). All calculated pathways (forwards and backwards) for each compound are presented in Tables S8–S19. The JOYSpectra web platform has proven to be a helpful tool for quantifying energy transfer rates. In a notable application, the JOYSpectra was utilized by Zhang, Wang, Xu et al. to elucidate the near 100% energy transfer efficiency from Uranyl to Eu^{3+} in a heterobimetallic metal-organic framework [75].

The IET results indicate that both forward and backward rates from the S_1 and T_1 channels are in the order of $\sim 10^8$ s^{-1}, as indicated in Fig. 6. Thus, there is no predominance of one channel suggesting that both are important in the IET processes. Such behavior is not commonly observed [16,17]. Although both S_1 and T_1 channels are operative in the present case, the T_1 channel is more significant when considering the total balance using a rate equations model. This is because the intersystem crossing rates ($S_1 \rightarrow T_1$ and $T_1 \rightarrow S_0$) have a crucial role in population kinetics [11]. It is worth highlighting that the exchange mechanism (W_{ex}, Eq. S10) has a major influence on the W^S, W^T, W_b^S and W_b^T rates.

Table 2 shows the total forward (W^S and W^T) and backward (W_b^S and W_b^T) rates for each channel. The W^S rates are composed mainly of the $^7F_0 \rightarrow {}^5D_1$ and $^7F_1 \rightarrow {}^5G_2$ transitions (pathways 2 and 13 in Tables S8, S10, S12, S14, S16, and S18), with contributions of 58.0 ± 0.1% and 34.4 ± 0.1%, respectively. On the other hand, the backward transfer rate W_b^S is dominated only by the $^5G_2 \rightarrow {}^7F_1$ transition (pathway 13 in Tables S9, S11, S13, S15, S17, and S19), with a contribution of 95.7 ± 0.1% of the total W_b^S. The backward energy transfer rates involving the T_1 state (W_b^T) has a great contribution of the $^5D_1 \rightarrow {}^7F_0$ transition (pathway 18 in Tables S9, S11, S13, S15, S17, and S19), corresponding to 91.8 ± 0.2% of the total rate. Despite the predominant focus on the $^5D_0$, $^5D_1$, $^5D_2$, and $^5L_6$ energy levels of the Eu^{3+} ion, the literature generally overlooks the involvement of other levels, such as the $^5G_2$, in the sensitization of Eu^{3+}. The $^5G_2$ state is crucial in the energy transfer process because it exclusively accepts energy through the exchange mechanism, specifically via the $^7F_1 \rightarrow {}^5G_2$ transition governed by selection rules on the total angular momentum quantum number J ($\Delta J = 0, \pm 1$). Additionally, once the population of the $^7F_1$ level is highly temperature-dependent according to Boltzmann statistics, it impacts directly the energy transfer through the $^7F_1 \rightarrow {}^5G_2$ pathway which can accept energy from both S_1 [76,77] and T_1 [11] states.

Table 2
Forward (W^S and W^T) and backward (W_b^S and W_b^T) IET rates (in s^{-1}) of the $C_n$mim[Eu(tta)$_4$] complexes (n = 3, 4, 5, 6, 7, and 8) obtained at 300 K.

Solid-state	W^S (s^{-1})	W^T (s^{-1})	W_b^S (s^{-1})	W_b^T (s^{-1})
C_3mim[Eu(tta)$_4$]	2.6×10^8	8.8×10^8	1.1×10^8	4.3×10^8
C_4mim[Eu(tta)$_4$]	2.6×10^8	3.0×10^8	1.1×10^8	4.2×10^8
C_5mim[Eu(tta)$_4$]	2.6×10^8	3.5×10^8	1.1×10^8	4.2×10^8
C_6mim[Eu(tta)$_4$]	2.6×10^8	3.1×10^8	1.1×10^8	4.2×10^8
C_7mim[Eu(tta)$_4$]	2.6×10^8	3.4×10^8	1.1×10^8	4.2×10^8
C_8mim[Eu(tta)$_4$]	2.6×10^8	4.4×10^8	1.1×10^8	4.2×10^8

Interestingly, the W^T rate has a different contribution from the $^7F_0 \rightarrow {}^5D_1$ and $^7F_1 \rightarrow {}^5D_0$ transitions (pathways 18 and 23 in Tables S8, S10, S12, S14, S16, and S18) depending on the energy barycenter of the T_1, this behavior is depicted in Fig. 7. Therefore, the higher the T_1 energy, the less participation of the $^7F_1 \rightarrow {}^5D_0$ pathway and the more participation of the $^7F_0 \rightarrow {}^5D_1$. These results are associated with the changing of the Δ (donor-acceptor energy difference) in Eq. S11, becoming more or less resonant with the energies of the $^7F_0 \rightarrow {}^5D_1$ and $^7F_1 \rightarrow {}^5D_0$ transitions.

The coordinates in the CIE (*Commission Internationale l'Eclairage*) chromaticity diagrams were determined based on the emission spectra of the $C_n$mim[Eu(tta)$_4$] and their corresponding $C_n$mim[Eu(tta)$_4$]@

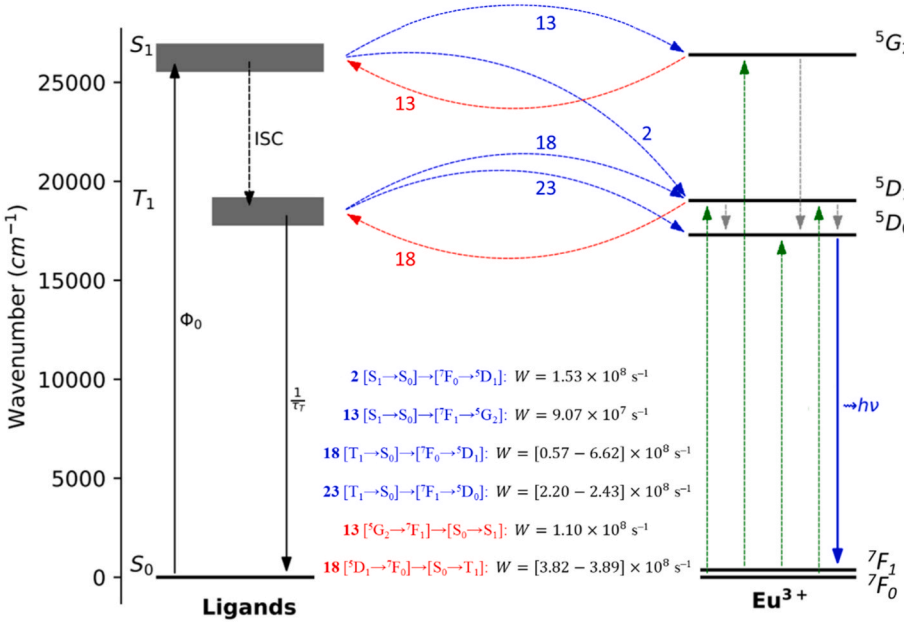

Fig. 6. Schematic Jablonski-type energy level diagram for the $[Eu(tta)_4]^-$ moieties. The barycenter of the S_1 (~26,250 cm^{-1}) and T_1 states (18,950–18,450 cm^{-1}, Table S3), respectively. S_0 is the tta fundamental level. Φ_0 is the pumping rate. ISC is the intersystem crossing $S_1 \rightsquigarrow T_1$ decay. Blue arrows represent the forward IET rate while the backward rates are the red ones. τ_T is the decay lifetime of the T_1 state. The gray dashed arrows are the non-radiative decay from higher levels of Eu^{3+} to the emitting one ($^5D_0$). This diagram was generated automatically from the JOYSpectra web platform [44].

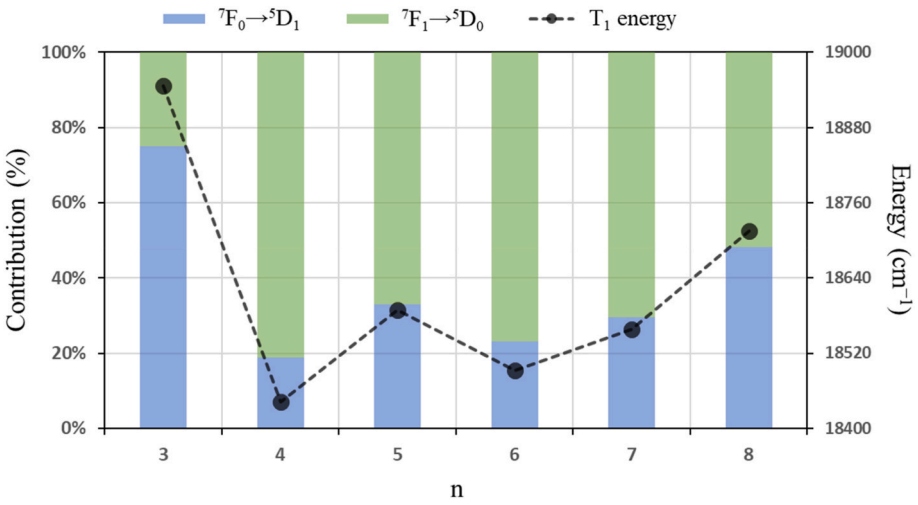

Fig. 7. Contributions of the two main energy transfer pathways involving the T_1: the $^7F_0 \rightarrow {}^5D_1$ (blue bars) and $^7F_1 \rightarrow {}^5D_0$ (green bars). The energies of the T_1 barycenters (right-side scale) are indicated by black dots.

[$C_n$mim]Br (n = 3 to 8) solutions under excitation at 365 nm at room temperature (Fig. 8). All [x,y] coordinates for both systems are very similar (Table S4) and located in the red region, revealing a highly monochromatic character. Fig. 8 also shows the digital camera photographs of the complexes in solid state and solution under ambient light and excited under 365 nm.

5. Conclusions

A series of lanthanide tetrakis complexes $C_n$mim[Ln(tta)$_4$] (Ln: Eu and Gd), with n = 3 to 8, were successfully synthesized and characterized. Phosphorescence spectra of the solid-state $C_n$mim[Gd(tta)$_4$] complexes showed that the T_1 state (~18,700 cm^{-1}) is barely affected by the carbon chain size (n). However, the experimental intensity parameters Ω_λ revealed some trends, although not very pronounced among the systems containing lower (n = 3 and 4) and higher (n = 6 and 7) numbers of carbons in $[C_n mim]^+$. In particular, the higher Q_{Eu}^{Eu} values found for the C_7mim[Eu(tta)$_4$] and C_8mim[Eu(tta)$_4$] complexes mainly reflect the significant decrease in the non-radiative rate (A_{nrad}). A systematic trend was not observed for the complexes in ionic liquid solutions. The high Ω_2 values either for the solid or solution samples corroborate with the intensity of the $^5D_0 \rightarrow {}^7F_2$ transition while the values of Ω_4 (associated with the $^5D_0 \rightarrow {}^7F_4$ transition) present more similarity among the series. The former has been demonstrated to be much more sensitive to angular variations (concerning Ω_4 and Ω_6), while Ω_4 is more affected by the Ln–O bond length [71,78].

The intramolecular energy transfer rates (calculated using the JOY-Spectra program [44]) for the solid-state compounds showed that both channels via S_1 and T_1 are operative, providing rates in the order of 10^8 s^{-1}. This behavior is not commonly observed in the literature [16,17], but it can be explained by the exceptional resonance between S_1 and T_1 with the $^5G_2$ and $^5D_0/{}^5D_1$ levels of the Eu^{3+}, respectively. It was demonstrated theoretically that the sensitization via T_1 may change the contribution of the IET rates to $^5D_{1,0}$ (starting from the $^7F_{0,1}$) according to the T_1 energy when n changes, as depicted in Fig. 7.

The Eu^{3+} tetrakis complexes revealed, in general, relatively high intrinsic quantum yields. The C_7mim[Eu(tta)$_4$] presents the highest values of Q_{Eu}^{Eu} = 90 and 86% in the solid-state and ionic liquid solution, respectively. In addition, all complexes present a highly red monochromatic emission either in a solid state or in solution as well as good thermal stability, being potential candidates for luminescent applications.

Author statement

T. B. Paolini: Conceptualization, Data curation, Writing – original draft, Visualization. **I. P. Assunção**: Data curation, Writing – original draft, Visualization. **I. F. Costa**: Investigation, Methodology, Data

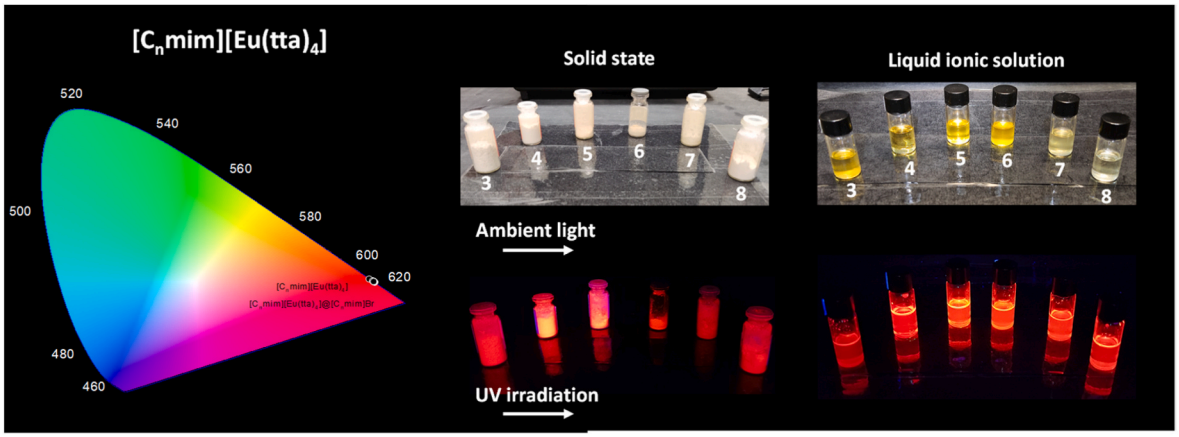

Fig. 8. The CIE diagram for the $C_n$mim[Eu(tta)$_4$] complexes and their corresponding $C_n$mim[Eu(tta)$_4$]@[$C_n$mim]Br ($3 \leq n \leq 8$) solutions from the emission spectra of both systems excited at 365 nm at room temperature. Photographs of the complexes in solid state and their corresponding solutions were taken with a digital camera under ambient light and excitation at 365 nm.

curation, Writing – original draft. **L. Blois**: Investigation, Methodology, Data curation, Writing – review & editing. **M. C. F. C. Felinto**: Conceptualization, Writing – original draft. **R. T. Moura Jr.**: Investigation, Methodology, Visualization, Writing – review & editing. **E.E.S Teotonio**: Investigation, Data curation, Writing – original draft, Visualization. **O.L. Malta**: Conceptualization, Writing – original draft. **A. N. Carneiro Neto**: Investigation, Methodology, Validation, Visualization, Formal analysis, Software, Writing – review & editing, Supervision. **H. F. Brito**: Conceptualization, Investigation, Data curation, Writing – original draft, Visualization, Supervision.

Declaration of competing interest

The authors declare that they have no known competing financial interests or personal relationships that could have appeared to influence the work reported in this paper.

Data availability

Data will be made available on request.

Acknowledgments

The authors are grateful to the Brazilian funding agencies CNPq and FAPESP for financial support. H.F. Brito is grateful to FAPESP (21/081110-2 and 21/08111-2) and CNPq for the research grant (306951/2018-5). This work was developed within the scope of the projects CICECO-Aveiro Institute of Materials, UIDB/50011/2020, UIDP/50011/2020 & LA/P/0006/2020, The Shape of Water (PTDC/NAN-PRO/3881/2020), and LogicALL (PTDC/CTM-CTM/0340/2021) financed by national funds through the FCT/MCTES (PIDDAC). E.E.S. Teotonio thanks the Universidade Federal da Paraíba (PVA13345-2020) for financial support. I.F. Costa thanks FAPESP (2022/12709-3) for his fellowship.

Appendix A. Supplementary data

Supplementary data to this article can be found online at https://doi.org/10.1016/j.jlumin.2023.120158.

References

[1] A.N. Carneiro Neto, E.E.S. Teotonio, G.F. de Sá, H.F. Brito, J. Legendziewicz, L. D. Carlos, M.C.F.C. Felinto, P. Gawryszewska, R.T. Moura Jr., R.L. Longo, W. M. Faustino, O.L. Malta, Modeling intramolecular energy transfer in lanthanide chelates: a critical review and recent advances, in: J.-C.G. Bünzli, V.K. Pecharsky (Eds.), Handb. Phys. Chem. Rare Earths, vol. 56, Elsevier, 2019, pp. 55–162, https://doi.org/10.1016/bs.hpcre.2019.08.001.

[2] L. Smentek, Lanthanides caged by the organic chelates; Structural properties, J. Phys. Condens. Matter 23 (2011), https://doi.org/10.1088/0953-8984/23/14/143202.

[3] S.I. Weissman, Intramolecular energy transfer - the fluorescence of complexes of europium, J. Chem. Phys. 10 (1942) 214–217, https://doi.org/10.1063/1.1723709.

[4] S. Sato, M. Wada, Relations between intramolecular energy transfer efficiencies and triplet state energies in rare earth β-diketone chelates, Bull. Chem. Soc. Jpn. 43 (1970) 1955–1962, https://doi.org/10.1246/bcsj.43.1955.

[5] A. Bellusci, G. Barberio, A. Crispini, M. Ghedini, M. La Deda, D. Pucci, Synthesis and luminescent properties of novel lanthanide(III) β-diketone complexes with nitrogen p,p'-disubstituted aromatic ligands, Inorg. Chem. 44 (2005) 1818–1825, https://doi.org/10.1021/ic048951r.

[6] N. Filipescu, W.F. Sager, F.A. Serafin, Substituent effects on intramolecular energy transfer. II. Fluorescence spectra of europium and Terbium β-diketone chelates, J. Phys. Chem. 68 (1964) 3324–3346, https://doi.org/10.1021/j100793a039.

[7] S.M. Bruno, R.A.S. Ferreira, F.A. Almeida Paz, L.D. Carlos, M. Pillinger, P. Ribeiro-Claro, I.S. Gonçalves, Structural and photoluminescence studies of a europium(III) tetrakis(β-diketonate) complex with Tetrabutylammonium, imidazolium, pyridinium and silica-supported imidazolium counterions, Inorg. Chem. 48 (2009) 4882–4895, https://doi.org/10.1021/ic900274a.

[8] R.D. Adati, M.R. Davolos, M. Jafelicci, S.A.M. Lima, C. Viegas, New phosphinate ligand synthesis and its effect on optical properties of the europium β-diketonate complex, Phys. Status Solidi Curr. Top. Solid State Phys. 6 (2009) 7–10, https://doi.org/10.1002/pssc.200881302.

[9] K. Binnemans, Rare-earth beta-diketonates, in: J.K.A. Gschneidner, J.-C.G. Bünzli, V.K. Pecharsky (Eds.), Handb. Phys. Chem. Rare Earths, Elsevier, 2005, pp. 107–272, https://doi.org/10.1016/S0168-1273(05)35003-3.

[10] H.F. Brito, O.M.L. Malta, M.C.F.C. Felinto, E.E.S. Teotonio, Luminescence phenomena involving metal enolates, in: J. Zabicky (Ed.), Chem. Met. Enolates, Wiley-VCH Verlag GmbH, Weinheim, Germany, 2009, pp. 131–177, https://doi.org/10.1002/9783527615858.

[11] A.N. Carneiro Neto, R.T. Moura, L.D. Carlos, O.L. Malta, M. Sanadar, A. Melchior, E. Kraka, S. Ruggieri, M. Bettinelli, F. Piccinelli, Dynamics of the energy transfer process in Eu(III) complexes containing polydentate ligands based on pyridine, Quinoline, and Isoquinoline as Chromophoric antennae, Inorg. Chem. 61 (2022) 16333–16346, https://doi.org/10.1021/acs.inorgchem.2c02330.

[12] A.J.S. Valentine, X. Li, Intersystem crossings in late-row elements: a perspective, J. Phys. Chem. Lett. 13 (2022) 3039–3046, https://doi.org/10.1021/acs.jpclett.2c00207.

[13] M. Kleinerman, Energy migration in lanthanide chelates, J. Chem. Phys. 51 (1969) 2370–2381, https://doi.org/10.1063/1.1672355.

[14] O.L. Malta, Ligand—rare-earth ion energy transfer in coordination compounds. A theoretical approach, J. Lumin. 71 (1997) 229–236, https://doi.org/10.1016/S0022-2313(96)00126-3.

[15] G.E. Buono-core, H. Li, B. Marciniak, Quenching of excited states by lanthanide ions and chelates in solution, Coord. Chem. Rev. 99 (1990) 55–87, https://doi.org/10.1016/0010-8545(90)80060-7.

[16] L.E. do N. Aquino, G.A. Barbosa, J. de L. Ramos, S.O.K. Giese, F.S. Santana, D. L. Hughes, G.G. Nunes, L. Fu, M. Fang, G. Poneti, A.N. Carneiro Neto, R.T. Moura, R.A.S. Ferreira, L.D. Carlos, A.G. Macedo, J.F. Soares, Seven-coordinate Tb^{3+} complexes with 90% quantum yields: high-performance examples of combined singlet- and triplet-to-Tb^{3+} energy-transfer pathways, Inorg. Chem. 60 (2021) 892–907, https://doi.org/10.1021/acs.inorgchem.0c03020.

[17] E. Kasprzycka, V.A. Trush, V.M. Amirkhanov, L. Jerzykiewicz, O.L. Malta, J. Legendziewicz, P. Gawryszewska, Contribution of energy transfer from the singlet state to the sensitization of Eu^{3+} and Tb^{3+} luminescence by sulfonylamidophosphates, Chem. Eur J. 23 (2017) 1318–1330, https://doi.org/10.1002/chem.201603767.

[18] R.T. Moura, J.A. Oliveira, I.A. Santos, E.M. Lima, L.D. Carlos, E.C. Aguiar, A.N. C. Neto, Theoretical evidence of the singlet predominance in the intramolecular energy transfer in ruhemann's purple Tb(III) complexes, Adv. Theory Simulations 4 (2021), 2000304, https://doi.org/10.1002/adts.202000304.

[19] I.M. Alaoui, Nonparticipation of the ligand's first triplet state in intramolecular energy transfer in Eu^{3+} and Tb^{3+} ruhemann's purple complexes, J. Phys. Chem. 99 (1995) 13280–13282, https://doi.org/10.1021/j100035a036.

[20] W.M. Faustino, G.F. De Sá, Intramolecular Energy Transfer through Charge Transfer State in Lanthanide Compounds : A Theoretical Approach Intramolecular Energy Transfer through Charge Transfer State in Lanthanide Compounds : A Theoretical Approach, 2005, 54109, https://doi.org/10.1063/1.1830452.

[21] J.J. Crosby, G.A. Whan, R.E. Freeman, Spectroscopic studies of rare earth chelates, J. Phys. Chem. 66 (1962) 2493–2499, https://doi.org/10.1021/j100818a041.

[22] R.E. Whan, G.A. Crosby, Luminescence studies of rare earth complexes: Benzoylacetonate and dibenzoylmethide chelates, J. Mol. Spectrosc. 8 (1962) 315–327, https://doi.org/10.1016/0022-2852(62)90031-0.

[23] I. Malina, V. Kampars, S. Belyakov, Dyes and Pigments Luminescence properties of 2-benzoyl-1,3-indandione based Eu^{3+} ternary and tetrakis complexes and their polymer films, Dyes Pigments 159 (2018) 655–665, https://doi.org/10.1016/j.dyepig.2018.07.003.

[24] A. Mech, M. Karbowiak, C. Görller-Walrand, R. Van Deun, The luminescence properties of three tetrakis dibenzoylmethane europium(III) complexes with different counter ions, J. Alloys Compd. 451 (2008) 215–219, https://doi.org/10.1016/j.jallcom.2007.05.019.

[25] R. Adati, J. Monteiro, L. Cardoso, D. de Oliveira, M. Jafelicci, M. Davolos, The influence of different ammonium cations on the optical properties of tetrakis Gd^{III} and Eu^{III} complexes, J. Braz. Chem. Soc. 30 (2019) 1707–1716, https://doi.org/10.21577/0103-5053.20190073.

[26] L. Margenfeld, P. Liebing, F. Oehler, V. Lorenz, F. Engelhardt, L. Hilfert, S. Busse, F. T. Edelmann, Two new series of potentially Triboluminescent lanthanide(III) β-diketonate complexes, Zeitschrift Für Anorg. Und Allg. Chemie. 644 (2018) 1177–1184, https://doi.org/10.1002/zaac.201800244.

[27] R. Ilmi, D. Zhang, L. Tensi, H. Al-Sharji, N.K. Al Rasbi, A. Macchioni, L. Zhou, W. Wong, P.R. Raithby, M.S. Khan, Salts of lanthanide(III) Hexafluoroacetylacetonates [Ln = Sm(III), Eu(III) and Tb(III)] with dipyridylammonium cations: synthesis, characterization, photophysical properties and OLED fabrication, Dyes Pigments 203 (2022), 110300, https://doi.org/10.1016/j.dyepig.2022.110300.

[28] S.-F. Tang, C. Lorbeer, X. Wang, P. Ghosh, A.-V. Mudring, Highly luminescent salts containing well-shielded lanthanide-centered complex anions and Bulky imidazolium countercations, Inorg. Chem. 53 (2014) 9027–9035, https://doi.org/10.1021/ic500979p.

[29] L.B. Guimarães, A.M.P. Botas, M.C.F.C. Felinto, R.A.S. Ferreira, L.D. Carlos, O. L. Malta, H.F. Brito, Highly sensitive and precise optical temperature sensors based on new luminescent Tb^{3+}/Eu^{3+} tetrakis complexes with imidazolic counterions, Mater. Adv. 1 (2020) 1988–1995, https://doi.org/10.1039/D0MA00201A.

[30] J.L. Lunkley, D. Shirotani, K. Yamanari, S. Kaizaki, G. Muller, Chiroptical spectra of a series of tetrakis((+)-3-heptafluorobutylyrylcamphorato)lanthanide(III) with an encapsulated alkali metal ion: circularly polarized luminescence and absolute chiral structures for the Eu(III) and Sm(III) complexes, Inorg. Chem. 50 (2011) 12724–12732, https://doi.org/10.1021/ic201851r.

[31] Y.H. Pham, V.A. Trush, A.N. Carneiro Neto, M. Korabik, J. Sokolnicki, M. Weselski, O.L. Malta, V.M. Amirkhanov, P. Gawryszewska, Lanthanide complexes with N -phosphorylated carboxamide as UV converters with excellent emission quantum yield and single-ion magnet behavior, J. Mater. Chem. C 8 (2020) 9993–10009, https://doi.org/10.1039/D0TC01445A.

[32] E. Kasprzycka, A.N. Carneiro Neto, V.A. Trush, L. Jerzykiewicz, V.M. Amirkhanov, O.L. Malta, J. Legendziewicz, P. Gawryszewska, How minor structural changes generate major consequences in photophysical properties of RE coordination compounds; resonance effect, LMCT state, J. Rare Earths 38 (2020) 552–563, https://doi.org/10.1016/j.jre.2020.02.001.

[33] A. Bhattacharjee, J.A. Lopes-da-Silva, M.G. Freire, J.A.P. Coutinho, P.J. Carvalho, Thermophysical properties of phosphonium-based ionic liquids, Fluid Phase Equil. 400 (2015) 103–113, https://doi.org/10.1016/j.fluid.2015.05.009.

[34] H.D.B. Jenkins, Ionic liquids-an overview. https://doi.org/10.3184/003685011X13138407794135, 2011.

[35] K. Binnemans, Lanthanides and actinides in ionic liquids, compr. Inorg. Chem. II, (Second Ed. From Elem. to Appl. 2 (2013) 641–673, https://doi.org/10.1016/B978-0-08-097774-4.00228-X.

[36] P. Nockemann, E. Beurer, K. Driesen, R. Van Deun, K. Van Hecke, L. Van Meervelt, K. Binnemans, Photostability of a highly luminescent europium β-diketonate complex in imidazolium ionic liquids, Chem. Commun. (2005) 4354–4356, https://doi.org/10.1039/b506915g.

[37] A.V. Rudnev, Electrodeposition of lanthanides from ionic liquids and deep eutectic solvents, Russ. Chem. Rev. 89 (2020) 1463–1482, https://doi.org/10.1070/rcr4970.

[38] A.V. Mudring, S. Tang, Ionic liquids for lanthanide and actinide chemistry, Eur. J. Inorg. Chem. (2010) 2569–2581, https://doi.org/10.1002/ejic.201000297.

[39] S. Samikkanu, K. Mellem, M. Berry, P.S. May, Luminescence properties and water coordination of Eu^{3+} in the Binary solvent mixture water/1-butyl-3-methylimidazolium chloride, Inorg. Chem. 46 (2007) 7121–7128, https://doi.org/10.1021/ic070329m.

[40] S. Arenz, A. Babai, K. Binnemans, K. Driesen, R. Giernoth, A.V. Mudring, P. Nockemann, Intense near-infrared luminescence of anhydrous lanthanide(III) iodides in an imidazolium ionic liquid, Chem. Phys. Lett. 402 (2005) 75–79, https://doi.org/10.1016/j.cplett.2004.12.008.

[41] M. Matsumoto, K. Takeuchi, Y. Inoue, K. Tsunashima, H. Yamada, Molecular Insight into the Ionic Conduction of Quaternary Ammonium and Phosphonium Cation-Based Ionic Liquids Using Dielectric and Spectroscopy Analyses, 2022, https://doi.org/10.1021/acs.jpcb.2c06110.

[42] H. Hakkou, J.J. Vanden Eynde, J. Hamelin, J.P. Bazureau, Ionic liquid phase organic synthesis (IoLiPOS) methodology applied to the three component preparation of 2-thioxo tetrahydropyrimidin-4-(1H)-ones under microwave dielectric heating, Tetrahedron 60 (2004) 3745–3753, https://doi.org/10.1016/j.tet.2004.03.026.

[43] M. Stalpaert, N. Peeters, D. De Vos, Conversion of lactide to acrylic acid by a phosphonium ionic liquid and acid cocatalyst, Catal. Sci. Technol. 8 (2018) 1468–1474, https://doi.org/10.1039/c7cy02364b.

[44] R.T. Moura Jr., A.N. Carneiro Neto, E.C. Aguiar, C.V. Santos Jr., E.M. de Lima, W. M. Faustino, E.E.S. Teotonio, H.F. Brito, M.C.F.C. Felinto, R.A.S. Ferreira, L. D. Carlos, R.L. Longo, O.L. Malta, (INVITED) JOYSpectra: a web platform for luminescence of lanthanides, Opt. Mater. X. 11 (2021), 100080, https://doi.org/10.1016/j.omx.2021.100080.

[45] R.S. Varma, V.V. Namboodiri, An expeditious solvent-free route to ionic liquids using microwaves, Chem. Commun. (2001) 643–644, https://doi.org/10.1039/b101375k.

[46] H.F. Brito, O.L. Malta, C.A. Alves De Carvalho, J.F.S. Menezes, L.R. Souza, R. Ferraz, Luminescence behavior of Eu^{3+} with thenoyltrifluoroacetonate, sulfoxides and macrocyclics, J. Alloys Compd. 275–277 (1998) 254–257, https://doi.org/10.1016/S0925-8388(98)00315-6.

[47] J.C. Dumke, B. El-Zahab, S. Challa, S. Das, L. Chandler, M. Tolocka, D.J. Hayes, I. M. Warner, Lanthanide-based luminescent nanoGUMBOS, Langmuir 26 (2010) 15599–15603, https://doi.org/10.1021/la102354h.

[48] M.S. Gruzdev, L.M. Ramenskaya, U.V. Chervonova, R.S. Kumeev, Preparation of 1-butyl-3-methylimidazolium salts and study of their phase behavior and intramolecular intractions, Russ. J. Gen. Chem. 79 (2009) 1720–1727, https://doi.org/10.1134/S1070363209080246.

[49] J.D. Holbrey, W.M. Reichert, R.P. Swatloski, G.A. Broker, W.R. Pitner, K.R. Seddon, R.D. Rogers, Efficient, halide free synthesis of new, low cost ionic liquids: 1,3-dialkylimidazolium salts containing methyl- and ethyl-sulfate anions, Green Chem. 4 (2002) 407–413, https://doi.org/10.1039/b204469b.

[50] A.R. Nekoei, S.F. Tayyari, M. Vakili, S. Holakoei, A.H. Hamidian, R.E. Sammelson, Conformation and vibrational spectra and assignment of 2-thenoyltrifluoroacetone, J. Mol. Struct. 932 (2009) 112–122, https://doi.org/10.1016/j.molstruc.2009.05.045.

[51] K. Nakamoto, Infrared and Raman Spectra of Inorganic and Coordination Compounds: Part A: Theory and Applications in Inorganic Chemistry, Wiley, Hoboken, NJ, USA, 2008, https://doi.org/10.1002/9780470405840.

[52] M.A. Guedes, T.B. Paolini, M.C.F.C. Felinto, J. Kai, L.A.O. Nunes, O.L. Malta, H. F. Brito, Synthesis, characterization and spectroscopic investigation of new tetrakis (acetylacetonato)thulate(III) complexes containing alkaline metals as countercations, J. Lumin. 131 (2011) 99–103, https://doi.org/10.1016/j.jlumin.2010.09.006.

[53] S. Cha, T. Shim, Y. Ouchi, D. Kim, Characteristics of visible fluorescence from ionic liquids, J. Phys. Chem. B 117 (2013) 10818–10825, https://doi.org/10.1021/jp4006313.

[54] W.T. Carnall, G.L. Goodman, K. Rajnak, R.S. Rana, A systematic analysis of the spectra of the lanthanides doped into single crystal LaF_3, J. Chem. Phys. 90 (1989) 3443–3457, https://doi.org/10.1063/1.455853.

[55] R.D. Shannon, C.T. Prewitt, Effective ionic radii in oxides and fluorides, Acta Crystallogr. Sect. B Struct. Crystallogr. Cryst. Chem. 25 (1969) 925–946, https://doi.org/10.1107/S0567740869003220.

[56] R.D. Shannon, Revised effective ionic radii and systematic studies of Interatomic distances in Halides and chalcogenides, Acta Crystallogr., Sect. A 32 (1976) 751–767, https://doi.org/10.1107/S0567739476001551.

[57] M. de Jong, L. Seijo, A. Meijerink, F.T. Rabouw, Resolving the ambiguity in the relation between Stokes shift and Huang–Rhys parameter, Phys. Chem. Chem. Phys. 17 (2015) 16959–16969, https://doi.org/10.1039/C5CP02093J.

[58] E. Kasprzycka, A.N. Carneiro Neto, V.A. Trush, O.L. Malta, L. Jerzykiewicz, V. M. Amirkhanov, J. Legendziewicz, P. Gawryszewska, Spectroscopic aspects for the Yb^{3+} coordination compound with a large energy gap between the ligand and Yb^{3+} excited states, Spectrochim. Acta Part A Mol. Biomol. Spectrosc. 274 (2022), 121072, https://doi.org/10.1016/j.saa.2022.121072.

[59] L. Blois, A.N. Carneiro Neto, O.L. Malta, H.F. Brito, A theoretical framework for optical thermometry based on excited-state absorption and lifetimes of Eu^{3+} compounds, J. Lumin. 249 (2022), 119039, https://doi.org/10.1016/j.jlumin.2022.119039.

[60] V. Trannoy, A.N. Carneiro Neto, C.D.S. Brites, L.D. Carlos, H. Serier-Brault, Engineering of mixed Eu^{3+}/Tb^{3+} metal-organic frameworks luminescent Thermometers with Tunable sensitivity, Adv. Opt. Mater. 9 (2021), 2001938, https://doi.org/10.1002/adom.202001938.

[61] K. Binnemans, Interpretation of europium(III) spectra, Coord. Chem. Rev. 295 (2015) 1–45, https://doi.org/10.1016/j.ccr.2015.02.015.

[62] P.A. Tanner, Lanthanide luminescence in solids, in: P. Hänninen, H. Härmä (Eds.), Lanthan. Lumin. Springer Ser. Fluoresc., Methods Appl., vol. 7, Springer-Verlag, Berlin, Heidelberg, 2010, pp. 183–233, https://doi.org/10.1007/4243_2010_6.

[63] W.T. Carnall, H. Crosswhite, H.M. Crosswhite, Energy Level Structure and Transition Probabilities in the Spectra of the Trivalent Lanthanides in LaF_3, Argonne, IL, United States, 1978, https://doi.org/10.2172/6417825.

[64] Y. Yang, J. Li, X. Liu, S. Zhang, K. Driesen, P. Nockemann, K. Binnemans, Listening to lanthanide complexes: determination of the intrinsic luminescence quantum yield by nonradiative relaxation, ChemPhysChem 9 (2008) 600–606, https://doi.org/10.1002/cphc.200700658.

[65] J.-C.G. Bünzli, S. V Eliseeva, Basics of lanthanide photophysics, in: P. Hänninen, H. Härmä (Eds.), Lanthan. Lumin. Photophysical, Anal. Biol. Asp, vol. 7, Springer, Berlin, Heidelberg, 2010, pp. 1–45, https://doi.org/10.1007/4243_2010_3.

[66] R.T. Moura Jr., A.N. Carneiro Neto, R.L. Longo, O.L. Malta, On the calculation and interpretation of covalency in the intensity parameters of 4f-4f transitions in Eu^{3+} complexes based on the chemical bond overlap polarizability, J. Lumin. 170 (2016) 420–430, https://doi.org/10.1016/j.jlumin.2015.08.016.

[67] A. Shyichuk, R.T. Moura, A.N.C. Neto, M. Runowski, M.S. Zarad, A. Szczeszak, S. Lis, O.L. Malta, Effects of dopant addition on lattice and luminescence intensity parameters of Eu(III)-Doped lanthanum Orthovanadate, J. Phys. Chem. C 120 (2016) 28497–28508, https://doi.org/10.1021/acs.jpcc.6b10778.

[68] N.S. Kariaka, V.A. Trush, V.V. Dyakonenko, S.V. Shishkina, S.S. Smola, N. V. Rusakova, T.Y. Sliva, P. Gawryszewska, A.N. Carneiro Neto, O.L. Malta, V. M. Amirkhanov, New luminescent lanthanide tetrakis-complexes $NEt_4[LnL_4]$ based on dimethyl-N-Benzoylamidophosphate, ChemPhysChem 23 (2022), https://doi.org/10.1002/cphc.202200129.

[69] G.B.V. Lima, J.C. Bueno, A.F. da Silva, A.N. Carneiro Neto, R.T. Moura, E.E. S. Teotonio, O.L. Malta, W.M. Faustino, Novel trivalent europium β-diketonate complexes with N-(pyridine-2-yl)amides and N-(pyrimidine-2-yl)amides as ancillary ligands: photophysical properties and theoretical structural modeling, J. Lumin. 219 (2020), 116884, https://doi.org/10.1016/j.jlumin.2019.116884.

[70] O.L. Malta, H.F. Brito, J.F.S. Menezes, F.R.G. e Silva, S. Alves, F.S. Farias, A.V.M. de Andrade, Spectroscopic properties of a new light-converting device Eu (thenoyltrifluoroacetonate)$_3$ 2(dibenzyl sulfoxide). A theoretical analysis based on structural data obtained from a sparkle model, J. Lumin. 75 (1997) 255–268, https://doi.org/10.1016/S0022-2313(97)00107-5.

[71] I.F. Costa, L. Blois, A.N. Carneiro Neto, E.E.S. Teotonio, H.F. Brito, L.D. Carlos, M. C.F.C. Felinto, R.T. Moura Jr., R.L. Longo, W.M. Faustino, O.L. Malta, in: M.G. Brik, A.M. Srivastava (Eds.), Chapter 2 Reinterpreting the Judd–Ofelt Parameters Based on Recent Theoretical Advances, first ed.Lumin. Mater., De Gruyter, 2023, pp. 19–62, https://doi.org/10.1515/9783110607871-002.

[72] A.V.S. Lourenço, C.A. Kodaira, E.M. Ramos-Sanchez, M.C.F.C. Felinto, H. Goto, M. Gidlund, O.L. Malta, H.F. Brito, Luminescent material based on the [Eu $(TTA)_3(H_2O)_2$] complex incorporated into modified silica particles for biological applications, J. Inorg. Biochem. 123 (2013) 11–17, https://doi.org/10.1016/j.jinorgbio.2013.02.006.

[73] R.O. Freire, A.M. Simas, Sparkle/PM6 parameters for all lanthanide Trications from La(III) to Lu(III), J. Chem. Theor. Comput. 6 (2010) 2019–2023, https://doi.org/10.1021/ct100192c.

[74] J.J.P. Stewart, Optimization of parameters for semiempirical methods V: modification of NDDO approximations and application to 70 elements, J. Mol. Model. 13 (2007) 1173–1213, https://doi.org/10.1007/s00894-007-0233-4.

[75] Y. Zhang, X. Wang, K. Xu, F. Zhai, J. Shu, Y. Tao, J. Wang, L. Jiang, L. Yang, Y. Wang, W. Liu, J. Su, Z. Chai, S. Wang, Near-Unity Energy Transfer from Uranyl to Europium in a Heterobimetallic Organic Framework with Record-Breaking Quantum Yield, 2023, https://doi.org/10.1021/jacs.3c01968.

[76] J.L. Moura, I.F. Costa, P.R.S. Santos, I.F. Silva, R.T. Moura, A.N. Carneiro Neto, W. M. Faustino, H.F. Brito, J.R. Sabino, E.E.S. Teotonio, Enhancing the luminescence of Eu(III) complexes with the ruthenocene Organometallic unit as ancillary ligand,

Inorg. Chem. 61 (2022) 13510–13524, https://doi.org/10.1021/acs.inorgchem.2c02115.

[77] R.T. Moura, M. Quintano, C.V. Santos Jr., V.A.C.A. Albuquerque, E.C. Aguiar, E. Kraka, A.N. Carneiro Neto, Featuring a new computational protocol for the estimation of intensity and overall quantum yield in lanthanide chelates with applications to Eu(III) mercapto-triazole Schiff base ligands, Opt. Mater. X. 16 (2022), 100216, https://doi.org/10.1016/j.omx.2022.100216.

[78] B.R. Judd, Ionic transitions hypersensitive to environment, J. Chem. Phys. 70 (1979) 4830, https://doi.org/10.1063/1.437372.